Nanoscale Advances

ROYAL SOCIETY OF CHEMISTRY

PAPER

View Article Online
View Journal | View Issue

Cite this: *Nanoscale Adv.*, 2020, **2**, 1625

Enhanced avidin binding to lipid bilayers using PDP-PE lipids with PEG-biotin linkers†

Holly L. Birchenough,[a] Marcus J. Swann,[b] Egor Zindy,[a] Anthony J. Day[a] and Thomas A. Jowitt *[a]

Two of the most important aspects of lipid bilayers that have increased their popularity in the field of nanotechnology and biosensors are their fluid nature, which is highly beneficial in ensuring the spatial organization of attached molecules, and the relative ease in which they can be manipulated to change the surface chemistry. Here we have used two different types of functionalized lipids to study the interaction of avidin, which is a common approach to attach further ligands for study. We have tested the commonly used Biotinyl-Cap-PE lipids at different molar percentages and reveal that avidin is not evenly distributed, but forms what looks like clusters even at low percentage occupancy which hampers the level of avidin that can be associated with the surface. We have then successfully employed the novel strategy of using PDP-PE lipids which contain a reducible disulphide to which we added maleamide-PEG-biotin spacers of different lengths. There is a more even distribution of avidin on these layers and thereby increasing the amount and efficiency of avidin association. The reduced levels of avidin that was being associated with the Biotinyl-Cap-PE layers as compared to the PDP-PE lipids could be analysed with QCM-D and interferometry approaches, but it was only with SEEC microscopy that the reason for the reduced occupancy was resolved.

Received 22nd January 2020
Accepted 7th March 2020

DOI: 10.1039/d0na00060d

rsc.li/nanoscale-advances

Introduction

The utilization of lipid supports on sensor surfaces has increased dramatically over the last few years. One reason for this is the relative ease in which one can make a well-ordered layer that can be tailored to suit the needs of the experiment. These can be bilayers,[1–5] self-assembled monolayers[6,7] or supported/tethered bilayers, using the integration of other molecules as supports distancing the layer from the surface.[8,9] The adaptability of the approach has led to exciting new developments in bio-nanotechnology[10,11] and in the design of novel characterization methods for investigating membrane protein–lipid interactions and antimicrobial peptides.[3,12,13] Biomimetic lipid layers, as well as being adaptable, have the potential to deliver a surface that is less chemically reactive and with native biological properties thereby allowing researchers to study more complex systems.

Another reason for the rapid advance of lipid biosensor-based applications is the introduction of instrumentation capable of monitoring both the formation of the layers and subsequent interactions in real time; notable among these are quartz-crystal microbalances (QCM), ellipsometers and interferometers such as the Farfield dual polarisation interferometer (DPI). The deposition of simple lipid bilayers onto planar surfaces using these technologies is in the most part by vesicle fusion of small unilamellar vesicles onto silica surfaces with a percentage of the lipids substituted for ones that are suitable for the attachment of proteins or other macromolecules.[1,4,14–20] The majority of these approaches use a molar percentage of between 5 and 10% functionalized lipids, utilizing predominantly either biotin- or NTA-moieties. On non-lipid based sensor surfaces the most widely used methods of attachment to proteins are through alkanethiol self-assembled monolayers or carboxyl-modified sugars, which can both subsequently be modified with the molecule of interest *via* carbodiimide chemistry and reactive NHS-esters. It is interesting that these chemistries are not often implemented on lipid layers, perhaps due to the inherent difficulty of forming bilayers with the necessary carboxyl head-groups.[18] Avidin is a tetravalent biotin binding protein, with the affinity for biotin being one of the tightest known natural non-covalent molecular associations. Most of the family of related avidin molecules from different species, such as streptavidin have very similar affinity and they provide a convenient way of attaching molecules to surfaces. Being multi-valent, avidin molecules can attach to a biotin-modified surface and have 1–2 binding sites still available for attaching further biotin-modified molecules.[1] New ways of attaching biotin to proteins such as with the AviTag™ or by

[a]*Wellcome Trust Centre for Cell-Matrix Research, UK. E-mail: t.jowitt@manchester.ac.uk*

[b]*Swann Scientific Consulting Ltd, 110 Sandy Lane, Lymm WA13 9HR, UK*

† Electronic supplementary information (ESI) available. See DOI: 10.1039/d0na00060d

using the twin Strep-Tag system[21] and novel avidin molecules such as Captavidin™,[22] which allows efficient removal of the molecules from the surface for regeneration purposes, opens up more possibilities for biotin coated sensor surfaces. Exploitation of lipid bilayer systems for biosensor applications relies on the membrane remaining fluid and fully formed without any ruptures or perturbations and without overcrowding the surface, which will restrict lateral diffusion. Most research groups use an arbitrary value of functionalized lipids between 5 and 10% (molar concentration) because of the lack of information on the levels needed for optimal protein coverage and there is a need to understand whether the most common biotin functionalized lipid, Biotinyl-Cap PE, is in fact appropriate. Here we have investigated the use of two types of functionalized lipids with three different lengths of surface linkers and have used QCM-D, dual polarization interferometry and surface enhanced ellipsometric contrast (SEEC) microscopy to provide detailed information on the optimal concentrations of functional group required to either saturate a surface or to provide a surface that has a controlled and uniform layer. We show that the traditional Biotinyl-Cap PE (BC-PE) lipids are not optimal for binding avidin moieties to the surface of the bilayers and that these form lipid clusters not detectable using non-visual techniques. Instead we identify a thiol-based alternative PDP-PE, which can be modified with PEG-biotin linkers that has a greater avidin-binding capacity and do not form these apparent clusters on the surface. These results have important implications for future studies and biomimetic bilayer design.

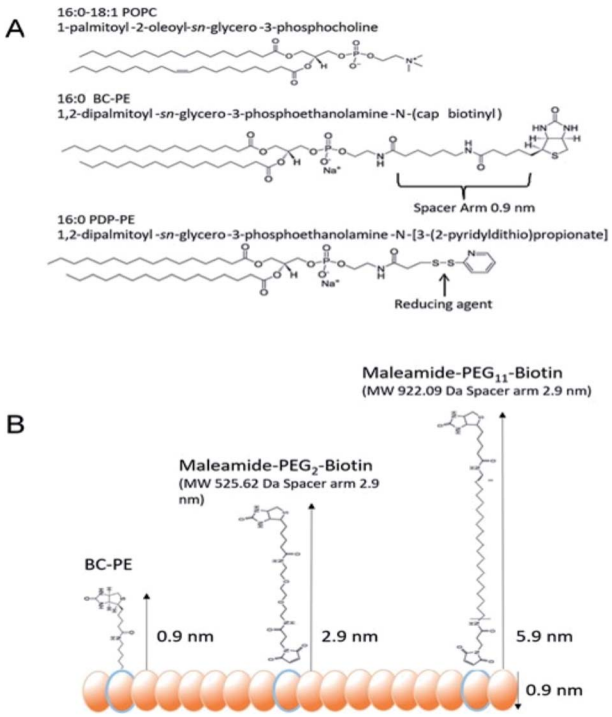

Fig. 1 (A) Lipids used in these experiments. (B) Biotinyl-Cap PE lipids (BC-PE) have a biotin group separated from the phosphoethanolamine group by a 0.9 nm spacer. The PDP-PE lipids have a reducible disulphide, which can be coupled with thiol reactive maleamide chemistry with PEG linkers of differing length. Here we have used 2-PEG and 11-PEG linkers between the ethanolamine groups and the biotin producing 2.9 nm and 5.9 nm spacing between the bilayer and avidin molecules.

Results

In order for us to investigate the effect of protein addition to the layers, and to study the effect of increasing the linker length between the protein and bilayer surface, we introduced varying percentages of 1,2-dipalmitoyl-*sn*-glycero-3-phosphoethanolamine-*N*-(Cap Biotinyl) herein called BC-PE and 1,2-dipalmitoyl-*sn*-glycero-3-phosphoethanolamine-*N*-(3-pyridinyldithio-propionate) referred to here as PDP-PE (Fig. 1A), lipids to the POPC liposomes. The BC-PE lipids contain a 0.9 nm spacer between the phosphoethanolamine and terminal biotin, whilst the PDP-PE has a reducible disulphide bond to which, following reduction, we were able to link maleamide-PEG-biotin linkers with either 2 or 11 polyethylene glycol (PEG) units creating 2.9 or 5.9 nm spacers (Fig. 1B). These lipids were incorporated at percentages of between 0.2–10% (molar concentration) of the total POPC lipid within the bilayer and it is assumed that there is an equal distribution of lipids throughout the two leaflets. Using DPI we analysed the change in birefringence of the layer after incorporation of the different head-groups. This showed a general decrease in lipid ordering with birefringence measurements dropping from 0.0210 ± 0.0003 to 0.0150 ± 0.0011. These small differences, whilst certainly detectable are within the range of birefringence measurements seen previously for full lipid bilayers[23] and indicate a small but detectable change in lipid anisotropy after incorporation of the functional lipid groups.

Following PDP-PE bilayer formation and reduction using TCEP, maleimide-PEG2-biotin and maleimide-PEG11-biotin linkers were incorporated. Mass addition of these molecules (526.62 Da and 922.09 Da, respectively) onto the surface was measured for each of the two linkers (at varying percentages of functionalised lipid relative to POPC) using DPI (Fig. 2). Total linker mass at equilibrium for each of the percentage points fits to a segmented linear approximation where the X^0 value of the upper plateau represents the level of layer saturation, and the intercept of the linear segments is the percentage at which total saturation is achieved. Not surprisingly larger mass addition was seen for maleimide-PEG11-biotin at ~0.22 ng mm^{-2} compared to ~0.15 ng mm^{-2} from maleimide-PEG2-biotin (Fig. 2A). The PEG11 layer saturated at ~2.1% functionalisation whereas the PEG2 layers saturated at ~3.9%. Using the average mass for each linker the number of molecules per mm^2 of the lipid surface was calculated as 1.5 and 1.6 × 10^{11} linker molecules per mm^2 at saturation for PEG11 and PEG2 respectively, indicating that there is little difference in the ability of each linker to immobilise to the functionalised lipid surface. At linker surface saturation, there is on average one linker present every 2.2 nm (PEG2) and 2.3 nm (PEG11) which is termed the molecular footprint (Fig. 2B). This also suggests that at saturation of the linkers *i.e.* ≥~2.1% functionalisation, there is molecular redundancy of binding sites. This means that there is

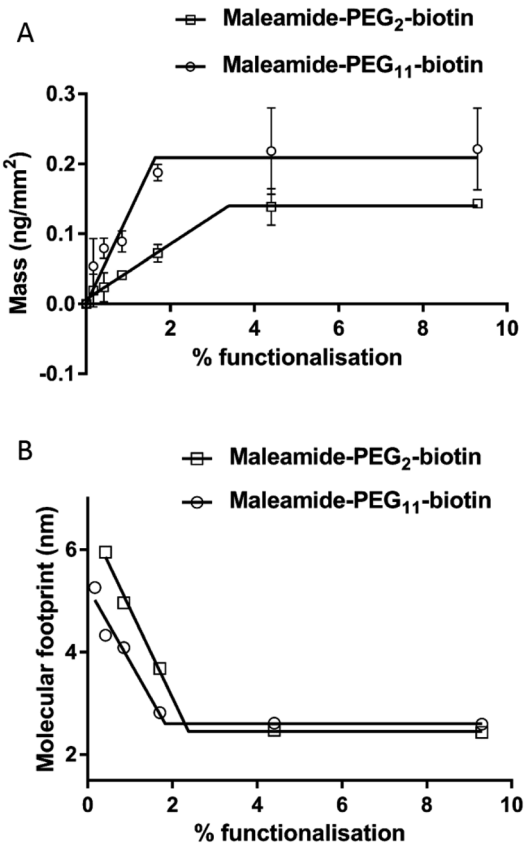

Fig. 2 Addition of maleamide-PEG-biotin linkers to the reduced PDP-PE lipids. (A) The mass of the linkers reaches a plateau of 2.2 ng mm^{-2} for the PEG11 linkers at 2% functionalisation and 1.5 ng mm^{-2} for the PEG2 linkers at 3.9% functionalisation. (B) Calculation of the molecular footprint, which is a measure of the area occupied by each linker, suggests that there is a linker present every ~2.1 nm in each direction.

no positive benefit in using higher percentages of functionalised lipid.

Avidin addition to the layers

In order to assess the ability of the layers to immobilise avidin, we first calculated the theoretical amounts of avidin that could be coupled in an idealised system using eqn (1):

$$\rho^{\text{surface}} = \frac{M}{(A \times N_A)} \quad (1)$$

where ρ^{surface} is the surface density, M is the molecular mass of avidin, in this case taken to be 66 kDa, and A is the surface area of avidin. This was calculated by measuring the hydrodynamic radius of avidin using dynamic light scattering (2.7 nm), which gives an effective maximal surface radius of 2.29×10^{-11} mm^2 for an equivalent sphere. If one assumes a random packing of non-overlapping spheres, which would give an approximation of maximal binding density in a diffusion limited system of 64%,[24] then the maximal surface coverage would be 3.1 ng mm^{-2}. Indeed if maximal non-random packing is achieved *via* free diffusion to form a 2D hexagonal lattice, this would give a packing density closer to 74% and a maximal surface density of 3.5 ng mm^{-2}. We also know from Fig. 2B that below ~2.1% PDP-PE the distance between linkers (or molecular footprint) is higher than the 2.7 nm (from avidin molecular dimensions) needed for close packing of avidin. Therefore, we can assume that all PDP-PE concentrations greater than 2.1% would give rise to saturation of the layers.

We compared the simulated avidin absorption for each of the linkers with the data recorded using DPI. Fig. 3 shows that all linkers followed the segmented linear approximations of the simulated data with X^0 values (the level of the upper plateau) corresponding to ~2% functionalisation at saturation. However, there are significant differences in the maximum level of avidin that can be bound to the surface. The BC-PE lipids (Fig. 3A) produced the lowest amount of protein mass addition of 1.60 ± 0.08 ng mm^{-2} at ~2% and a maximal amount of 2.10 ng mm^{-2} at 10%. PEG2-biotin layers (Fig. 3B) exhibited the greatest mass addition at 3.20 ± 0.10 ng mm^{-2} followed by PEG11-biotin layers saturating at approximately 2.70 ± 0.15 ng mm^{-2} (Fig. 3C). Surprisingly, we also observed the PEG11 linkers at percentages below 1% do not follow a linear response

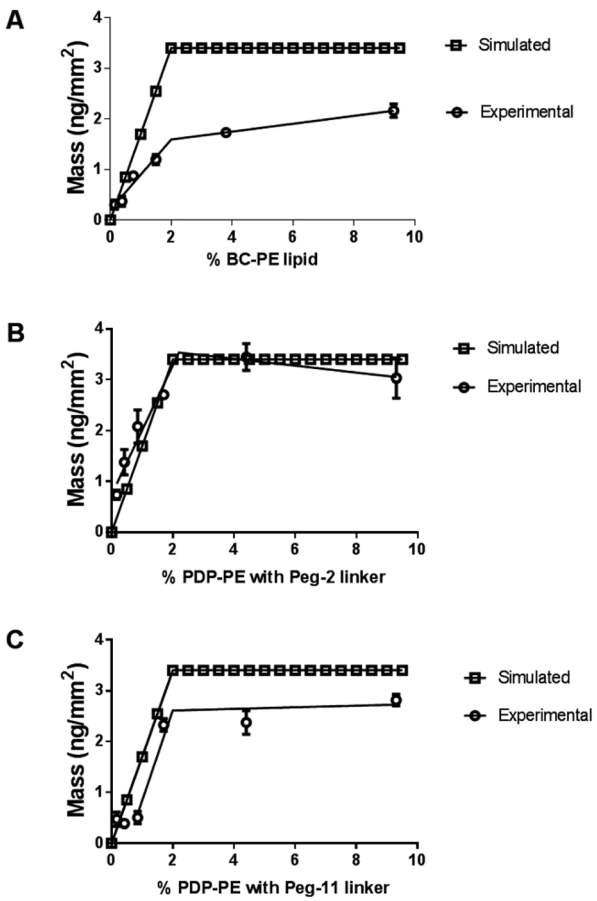

Fig. 3 Addition of avidin to the functionalised lipid layers. In each case the simulated data is based on avidin binding to saturation at each of the functionalised lipid percentages with a fixed saturation point of 2.3% is compared to real association data fitted to a segmental linear approximation with no fixed data points. (A) Addition of avidin to BC-PE lipids, (B) addition of avidin to PDP-PE with PEG2-biotin linkers and (C) to PDP-PE lipids with PEG11-biotin linkers.

but rather the shape of the curve is sigmoidal suggesting that at low percentages there are problems associated with biotin availability. Interestingly based on QCM-D measurements, quantitation of mass using the Sauerbrey equation estimated maximal bound mass of ~8 ng mm^{-2} for PEG2 and BC-PE and 6 ng mm^{-2} for the PEG11-linkers (ESI Fig. 1†). These higher total mass additions compared to DPI values are due to coupled water.[25,26] So it is apparent that the level of coupled water is greater for the BC-PE linker, at ~6.4 ng mm^{-2} water compared to values of 5.9 and 3.3 ng mm^{-2} for PEG2 and PEG11 respectively, and is inversely related to linker length. This highlights that when avidin is close to the surface, *i.e.* within 1–3 nm, the level of water associated with the layer is significantly higher. QCM-D measurements clearly distort the apparent amount of bound protein depending upon the length of the linker used. The shorter linkers trapping more bound water than the longer more flexible ones.

At low percentage functionalization there is a strong relationship between association rate and linker length (ESI Fig. 2†). BC-PE (0.9 nm spacer arm) has the slowest association rate at $1.1 \pm 0.3 \times 10^6$ M^{-1} min^{-1} at 1% functionalization. The PEG11-biotin surfaces (5.9 nm spacer arm) demonstrated an order of magnitude quicker on-rate ($1.1 \pm 0.2 \times 10^7$ M^{-1} min^{-1}) at low functionalization (0.2%). It can be concluded that at the lower percentage-functionalization the biotin is more readily available for binding when immobilised at greater distances from the lipid surface. Above ~2% functionalization, *i.e.* the level at which avidin saturation occurs, the association of avidin with both the PEG linkers is diffusion limited and restricted to ~5×10^6 M^{-1} min^{-1} but the BC-PE linkers fail to reach the association rates exhibited by the PEG linkers until much higher percentages.

Understanding the sigmoidal behaviour of avidin association to PEG11-biotin linkers

The average surface mass of immobilised avidin molecules is calculated to be ~3.2 ng mm^{-2} at saturation. This is consistent with an almost complete monolayer of closely packed avidin on the lipid surface. We have shown (Fig. 3) that both BC-PE and PEG11 saturate at levels lower than PEG2 and therefore we can assume that these immobilisation methods produce less densely packed surfaces and are unable to form complete monolayers. At low percentage functionalization (*i.e.* below 2%) the layers for BC-PE and PEG2-biotin exhibit linear mass/percentage responses that fit to the expected segmented linear approximation for molecular association. However, as shown in Fig. 3C and 4A, the PEG11-biotin layer exhibits very low avidin binding at low percentages. The sigmoidal binding curve for PEG11-biotin, which is most pronounced using DPI suggests that at low functionality, the biotin attached to the longer linker is potentially unavailable for binding. There is no evidence from the birefringence that the PEG11 linker is inserted into the bilayer (data not shown) but the lack of avidin binding would suggest that the linkers may be associated closely to the lipid surface and unavailable, or more than one linker is attached to one avidin molecule.

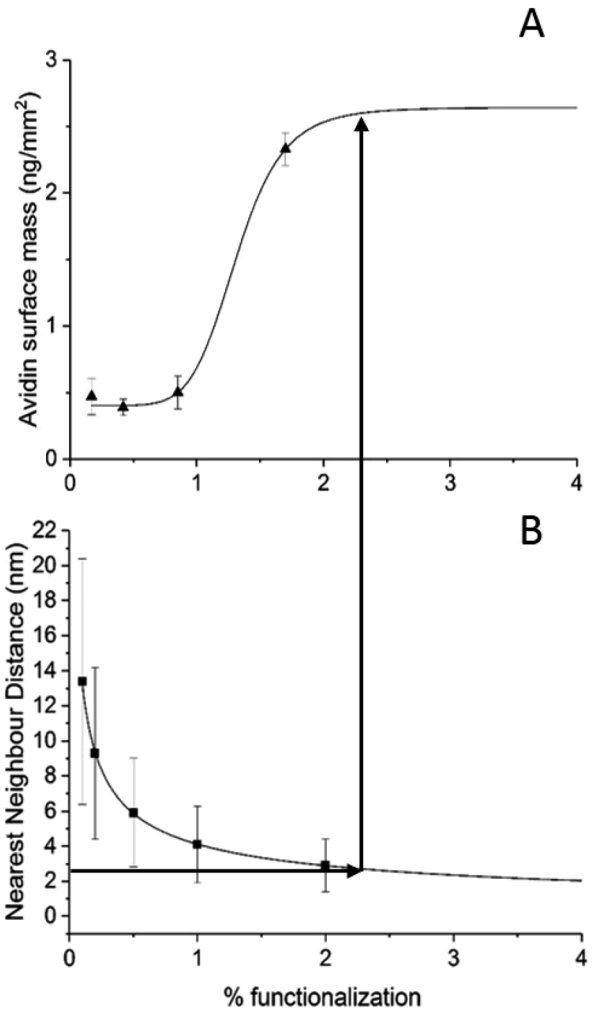

Fig. 4 (A) The availability of biotin binding sites at low percentages of PDP-PE for PEG11 linkers follows a sigmoidal pattern indicating that at percentages below 1% the longer linker is not available for binding. (B) Calculation of the nearest neighbour distribution of functionalised lipids indicates that when the distance between adjacent functionalised lipids falls below 2.5 nm there is a rapid increase in availability of the PEG11. This is the point at which molecular crowding of the linkers forces biotin availability.

To understand this phenomenon we simulated the nearest neighbour spatial distribution of functionalized lipids within the bilayer for each percentage of linker addition using the method of Clark and Evans, which has been adapted for use within the ImageJ software by Ciaran Beggan and Christopher Hamilton.[27] The simulation represents labelled/functionalised lipids within a planar bilayer in a random distribution within a known area (ESI Fig. 3†). Functionalized percentages of between 0.1% and 5% show that the neighbouring labelled lipids are on average 12.4 nm apart for 0.1% lipid layers, to 1.8 nm apart for 5% functionalised lipid layers. Based on the molecular footprint of avidin, interference by neighbouring attachment sites would start at levels above 1% functionalization. This is also the point at which we could start to see multivalency. However below this, the distance between linkers is too

great for multi-valency to be a significant problem assuming a random distribution of linkers. The interfering effects of neighbouring linkers, which for the PEG11-biotin have a footprint of 2.6 nm (Fig. 2B), becomes evident at >2% functionalisation. It seems therefore that the sigmoidal pattern observed for PEG11-biotin is caused by molecular crowding of the linkers. At concentrations higher than 2% functionalisation, linker availability is increased, likely due to self-assembly on the surface. At lower concentrations the lack of self-assembly leads to a decrease in biotin availability perhaps due to steric effects of the lipid surface. Interestingly, given the fast association of the avidin to the PEG11-biotin linkers (ESI Fig. 2†), those biotin moieties that are available become quickly bound to the avidin; however, the total mass of avidin on the surface is reduced compared to PEG2-biotin, most likely due to multiple occupancy of biotin binding sites.[1]

Using surface enhanced ellipsometric imaging to understand the lower avidin binding efficiency of the BC-PE lipid

In order to understand why we are seeing consistently lower avidin association to the BC-PE lipid we used a quantitative technique called time resolved Surface Enhanced Ellipsometric Contrast (SEEC) imaging. This technique, described by Frederik Hook's group in 2012 (ref. 28) and first developed by Ausserre and Valignat in 2007,[29] provides high-resolution imaging and thickness measurements in real-time on thin films. The SEEC sensors are used in the place of conventional microscope slides on a widefield microscope with a ×25 objective and are composed of multiple layers of organic oxides that produce a non-reflective surface under canonical illumination.[30] When material is deposited upon this surface, in our case using a microfluidics channel to achieve time-resolved measurements, the contrast enhancement is ~100-fold compared to that produced by non-enhanced widefield microscopy.[30] In addition to the enhancement in contrast, the thickness of the film can be accurately measured using the Fizeau fringes created by optical interference in the colorimetric range of the reflected light. Each pixel is converted into an optical thickness which is accurate over the range of approximately 0.1 nm to 200 nm based on the colour changes of a thickness standard.[30,31] We deposited POPC bilayers functionalised with PDP-PE and BC-PE lipids onto the surface of the SEEC sensors and captured image frames every 5 seconds. Using the Sarusoft software we were able to pick one or multiple areas for the analysis of thickness change throughout sequential frames as illustrated in Fig. 5. Instantaneous rupture of the lipids occurred in all cases and there was no evidence of membrane perturbations or gaps. The thickness of the layers was ~4.25 nm at saturation for all the lipids tested. Avidin was then added to the BC-PE (Fig. 5B) and PDP-PE lipids (following linker addition) (Fig. 5B), which showed remarkably different results. The BC-PE lipids exhibited the formation of areas of higher thickness that were not present on the PDP-PE lipids. These were evident from 0.2–10% functionalization (ESI Fig. 4†). Analysis of the thickness of the different zones showed that these zones were areas where avidin was more concentrated, presumably

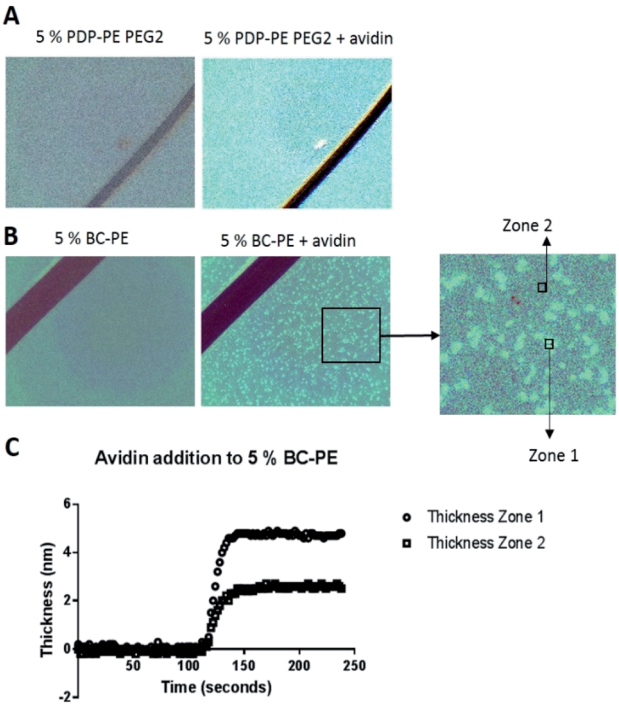

Fig. 5 SEEC microscopy. (A) A 5% PDP-PE bilayer with PEG2-linkers before and after avidin addition. The addition of avidin to the layer changes the colour of the image, which can be translated into a thickness measurement. In this case ~5 nm. (B) Addition of avidin to a 5% BC-PE layer reveals binding takes place in select areas of the layer. These clusters can be selected for analysis individually where Zone 1 is the brighter region and Zone 2 is the darker region. (C) The results show that avidin at ~5.5 nm binds in Zone 1, and not as densely in Zone 2.

because the BC-PE was more localized and evidenced by the ~5 nm change in thickness (Fig. 5C); in between the spots there was a contribution of avidin binding but at a lower level evidenced by the lower level of ~2.5 nm at 5% functionalisation. This highlights that the BC-PE lipids are forming larger clusters whereas the PDP-PE lipids do not, which therefore explains the reduction in avidin binding efficiency observed for BC-PE lipids.

Discussion

We have compared two different attachment strategies for the association of avidin molecules onto lipid bilayers. The first using biotin functionalized lipids (BC-PE), and the second using 1,2-dipalmitoyl-*sn*-glycero-3-phosphoethanolamine-*N*-[3-(2-pyridyldithio)-propionate] (PDP-PE) which is a novel approach to the attachment of molecules to layers using the reduced thiol. Adding a known percentage of biotinylated lipids and capturing avidin is the most common method for coupling proteins to lipid surfaces and has been used in many applications.[1,7,17,32–35] The use of PDP-PE is a method used here to link avidin to lipid bilayers *via* spacer intermediates. By using this approach we are able to modulate the length of the spacer and therefore the distance of the attached target molecule (in our case avidin) from the surface. We have shown that this enhances the

coupling of avidin molecules to the surface in both quantity and efficiency compared to the standard BC-PE method. Saturation occurred extremely rapidly for PEG11-linkers, slightly slower for the PEG2 but was an order of magnitude slower for BC-PE. Ouberai *et al.*[26] showed that lysozyme covered a bare SiO_2 surface with a density of 2.87 ng mm^{-2} and BSA, which has a similar size to avidin, with 1.83 ng mm^{-2} according to dry mass calculations using DPI measurements of proteins absorbed onto the surface. Interestingly when we use DPI to study the maximum level of addition of avidin onto the PDP-PE layers using the PEG2-biotin linker (corresponding to a 2.9 nm spacer; Fig. 1B), we obtained a surface coverage of 3.2 ± 0.1 ng mm^{-2} which is consistent with a complete monomeric layer. This suggests that the PEG2-biotin spacers are capable of forming a layer that has a significantly higher level of saturation compared to physisorption and is the same as the theoretical diffusion-limited maximal level of binding. This greater binding efficiency is likely due to the diffusional capability of the lipids.

BC-PE lipids, which have the shortest spacer arm, are the most common form of functionalized lipid used in the literature, but we have shown these to be far from ideal. This type of linker when bound to avidin couples large amounts of water to the lipid surface. Molecular modelling of avidin bound to the lipids (PDB files extracted from Dr Peter Tieleman's website, University of Calgary) by all three linkers (Fig. 6) indicates that the BC-PE linkers could create a substantial interaction between the avidin and the lipid surface creating a super-hydrated and rigidly coupled layer which fits with our data comparing surface coverage from the DPI and QCM-D, which suggests that there is far greater coupled water for the BC-PE lipids than the other linkers. The molecular model in Fig. 6 also indicate that avidin bound to BC-PE lipids interacts with the phosphatidylcholine head-group of the lipid surface. This could have the causative effect of altering lipid surface dynamics. The PEG11-biotin and PEG2-biotin linkers in contrast have much faster kinetics for their association to avidin presumably due to higher availability of the biotin. We have shown that the longer PEG11 linkers are not very good at binding avidin below concentrations of 2% but above this, the long linkers have increased availability. Our data from the simulation of nearest neighbour distributions suggests that this could be due to the longer PEG chains arranging in a self-assembled monolayer but we have no direct proof of this. Below 2% these longer linkers are not optimal for binding proteins to the surface. However for both the PEG2-biotin and PEG11-biotin linkers there is little difference in surface immobilized mass of avidin binding at percentage functionalization above 5%.

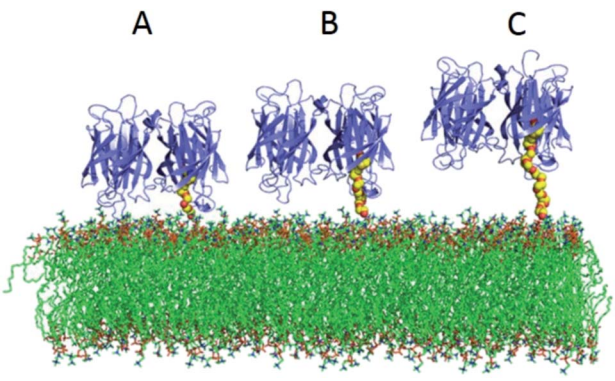

Fig. 6 Modelling the linkers as rigid/semi-rigid polymers of known length. (A) BC-PE, (B) PDP-PE PEG2 and (C) PDP-PE PEG11 on a POPC lipid bilayer. This suggests that when using Biotinyl-Cap PE, the avidin will interact with the lipid surface.

Most importantly we have found that BC-PE lipids produce what looks like surface clusters. These areas of higher avidin concentration can be clearly viewed using SEEC microscopy and the contrast interferometric responses for avidin binding within and outside of these clusters (Fig. 5B) indicates a clear difference in the levels of binding. This phenomenon explains the overall lower dry mass response to avidin association recorded using DPI compared to that of the PDP-PE lipids and the PEG2-biotin linkers. The reason that avidin is binding in areas of higher density is unclear. This could be due to clustering of the BC-PE lipids where the difference in charges of the BC-PE lipids cause local non-random associations and like-molecules may separate into these domains. It is also possible that this is due to membrane curvature,[36] but significant curvature was not observed in the membrane thickness measurements. However lateral pressure caused by changes in the packing of the BC-PE chains could cause differential pressure distributions[37] which causes membrane curvature that is not detected as changes in overall thickness but is sufficient to cause clustering of like-molecules. This could also be occurring in the PDP-PE but with much smaller clusters which do not adversely affect the levels of avidin that can be associated with the surface.

Conclusion

These results show that using BC-PE lipids will result in clustering of avidin molecules on the surface of the lipid layer and this can be resolved using PDP-PE lipids, to which one can add maleamide-PEG-biotin linkers. We also show that PEG2-biotin linkers bind the most avidin, have fast kinetics and have no deleterious effects on the layer itself. We have also shown that there is no effective need to use greater than 2.5% functionalised lipid. Higher percentages than this result in molecular redundancy of the linkers.

Experimental

Liposome preparation

Lyophilised 1-palmitoyl-2-oleoyl-*sn*-glycero-3-phosphocholine (POPC) was dissolved in chloroform, with or without head group-functionalized lipid (*i.e.* 1,2-dipalmitoyl-*sn*-glycero-3-phosphoethanolamine-*N*-(Cap biotinyl) (referred to here as BC-PE) or 1,2-dipalmitoyl-*sn*-glycero-3-phosphoethanolamine-*N*-[3-(2-pyridyldithio)propionate] (termed PDP-PE)) (Avanti Polar Lipids, USA), within a glass tube. Chloroform was removed under a continuous nitrogen stream to produce a thin lipid film. Tubes were placed under vacuum for a minimum of 2 h to ensure all chloroform had been removed. Lipid films were rehydrated in 20 mM HEPES, 150 mM NaCl, 2 mM $CaCl_2$, pH 7.4

at 1 mg ml^{-1}. Lipid solutions were extruded through a 50 nm pore size filter composed of polycarbonate membranes (Whatman®, GE Healthcare Life Sciences), using a mini-extruder set (Avanti Polar-Lipids, USA). Dynamic Light Scattering (DLS) using a Zetasizer nano-S instrument (Malvern Instruments Ltd, UK) was used to check the size of the unilamellar vesicles. Only vesicles producing single peaks with a *z*-average of approximately 100 nm and below were used.

QCM-D and DPI chip surface preparation

Q-sense (SiO_2) and Analight unmodified (SiO_xN_y) chips were treated to a surface cleaning process prior use, however Analight chips were cleaned approximately 12 h before use and Q-sense chips immediately before use. Chips were sonicated in 0.2% (w/v) SDS for 15 min and then rinsed extensively in ddH_2O. Surfaces were then rinsed in ethanol and dried under nitrogen. Chips were finally placed under UV Ozone (ProCleaner™ Plus, (Bioforce Nanosciences)) for 30 min. Q-sense chips were used immediately and Analight chips were stored dry until use.

Quartz crystal microbalance with dissipation monitoring (QCM-D)

QCM-D measurements were performed on a Q-sense E1 or a Q-sense Omega with standard flow module. All sample injections were undertaken in flow mode (continuous solution delivery to the measurement chamber) injecting 200 μl at 25 μl min^{-1}. Changes in dissipation (D) and normalised frequency (f) were measured in all overtones but are only displayed for the fifth overtone (25 MHz). For lipid bilayer production small unilamellar vesicles (SUVs) (100 μg ml^{-1}) were injected at 25 μl min^{-1} over pre-equilibrated SiO_2 Q-sense chips in filtered and degassed 20 mM HEPES, 150 mM NaCl, 2 mM $CaCl_2$, pH 7.4 at 21 °C. Following planar bilayer production, running buffer was changed to filtered and degassed 20 mM HEPES, 150 mM NaCl, pH 7.4 (RB). BSA (100 μg ml^{-1} in RB) was injected over formed bilayers at 50 μl min^{-1} to ensure continuous coverage. For experiments in which linkers were used, disulphide capped lipids (PDP-PE) were reduced with 10 mM tris(2-carboxyethyl) phosphine (TCEP) in RB injected over the lipid surface at a flow rate of 50 μl min^{-1} for a minimum of 10 minutes or until the response had plateaued. Linkers (EZ-Link® maleimide-PEG2-biotin or EZ-link® maleimide-PEG11-biotin (Thermo)) were re-suspended in RB at a concentration of 1 mM and flowed over the reduced lipid surface at a flow rate of 20 μl min^{-1} for a ~10 minutes or until the response had again plateaued. For the subsequent production of an avidin layer, 10 μg ml^{-1} of this protein was flowed over the bilayer surface at 50 μl min^{-1} in RB until the surface was saturated. Analysis of layers was performed using the Qtools software (Q-sense®, Sweden).

Dual polarization interferometry (DPI)

An Analight® dual polarization interferometer (DPI) (Analight® 4D, Farfield-Biolin Scientific AB, Sweden) was used to measure lipid bilayer production and protein addition. The instrument was set to 20 °C throughout all experiments. Cleaned chips were equilibrated in filtered and degassed 20 mM HEPES, 150 mM NaCl, 2 mM $CaCl_2$, pH 7.4 (RB) within the flow module for a minimum of 30 min. System calibrations were undertaken prior to each experiment which consisted of an injection of filtered and degassed 80% (w/w) ethanol for chip calibration followed by an injection of filtered and degassed ddH_2O for bulk calibrations. Only experimental set-ups that passed the calibration criteria were used. Lipid bilayer production was carried out as described for QCM-D experiments (see above) before buffer was changed for filtered and degassed RB. Avidin injections were performed as described for QCM-D with a 200 μl injection loop. Initial layer analysis was undertaken using the Analight® 4D Resolver software (Farfield-Biolin Scientific AB, Sweden). Lipid refractive index (RI) was set to 1.47 and the dn/dc to 0.135 (ref. 23) with thickness, mass and birefringence measurements unfixed. The dn/dc for protein analysis was set to a standard value of 0.182 and all remaining measurements were left unfixed unless otherwise stated within the Results section.

Surface enhanced interferometric microscopy

The N-Lab Station (Nanolane, France) was used to measure the real-time binding of avidin-containing bilayers to SEEC sensors. Lipids were produced in the same manner as for QCM-D and DPI. Silicon-dioxide wet Sarfus slides were used without any prior cleaning. Sarfus slides were inserted into the instrument and scratched to provide a focal point before the 1-channel fluidics system was assembled on top. Buffer (20 mM HEPES, 150 mM NaCl, 2 mM $CaCl_2$, pH 7.4) was flowed over at ~100 μl min^{-1} and the microscope was focused on the scratch using a 50× objective. Lipid deposition, reduction of PDP-PE, linker addition and avidin immobilisation were performed in the same manner as for DPI and QCM-D. Images were recorded every second at each phase of the experiment for example, lipid layer addition, reduction, linker addition and avidin deposition.

Dynamic light scattering

DLS measurements were performed with Zetasizer Nano-S (Malvern, Germany). The measurements of both lipid vesicles and avidin were taken in a 1 cm 45 μl quartz cuvette at a temperature of 20 °C. Avidin or vesicles were analysed at a concentration of 1 mg ml^{-1} taking three measurements of 13 averages each.

Conflicts of interest

There are no conflicts to declare.

Acknowledgements

We would like to thank the Biotechnology and Biological Sciences Research Council (BBSRC), Biolin Scientific and the Wellcome Trust for funding this project.

References

1 G. V. Dubacheva, C. Araya-Callis, A. Geert Volbeda, M. Fairhead, J. Codee, M. Howarth, *et al.*, Controlling

Multivalent Binding through Surface Chemistry: Model Study on Streptavidin, *J. Am. Chem. Soc.*, 2017, **139**(11), 4157–4167.

2 A. Sumino, T. Dewa, T. Takeuchi, R. Sugiura, N. Sasaki, N. Misawa, *et al.*, Construction and structural analysis of tethered lipid bilayer containing photosynthetic antenna proteins for functional analysis, *Biomacromolecules*, 2011, **12**(7), 2850–2858.

3 S. Forbes, A. J. McBain, S. Felton-Smith, T. A. Jowitt, H. L. Birchenough and C. B. Dobson, Comparative surface antimicrobial properties of synthetic biocides and novel human apolipoprotein E derived antimicrobial peptides, *Biomaterials*, 2013, **34**(22), 5453–5464.

4 O. Beutel, F. Roder, O. Birkholz, C. Rickert, H. J. Steinhoff, M. Grzybek, *et al.*, Two-Dimensional Trap for Ultrasensitive Quantification of Transient Protein Interactions, *ACS Nano*, 2015, **9**(10), 9783–9791.

5 D. Melendrez, T. Jowitt, M. Iliut, A. F. Verre, S. Goodwin and A. Vijayaraghavan, Adsorption and binding dynamics of graphene-supported phospholipid membranes using the QCM-D technique, *Nanoscale*, 2018, **10**(5), 2555–2567.

6 J. N. Barbosa, M. C. Martins, S. C. Freitas, I. C. Goncalves, A. P. Aguas and M. A. Barbosa, Adhesion of human leukocytes on mixtures of hydroxyl- and methyl-terminated self-assembled monolayers: effect of blood protein adsorption, *J. Biomed. Mater. Res., Part A*, 2010, **93**(1), 12–19.

7 N. Ballav, A. Terfort and M. Zharnikov, Fabrication of mixed self-assembled monolayers designed for avidin immobilization by irradiation promoted exchange reaction, *Langmuir*, 2009, **25**(16), 9189–9196.

8 R. Budvytyte, M. Mickevicius, D. J. Vanderah, F. Heinrich and G. Valincius, Modification of tethered bilayers by phospholipid exchange with vesicles, *Langmuir*, 2013, **29**(13), 4320–4327.

9 R. Budvytyte, G. Valincius, G. Niaura, V. Voiciuk, M. Mickevicius, H. Chapman, *et al.*, Structure and properties of tethered bilayer lipid membranes with unsaturated anchor molecules, *Langmuir*, 2013, **29**(27), 8645–8656.

10 T. Albrecht, Nanobiotechnology: a new look for nanopore sensing, *Nat. Nanotechnol.*, 2011, **6**(4), 195–196.

11 E. C. Yusko, J. M. Johnson, S. Majd, P. Prangkio, R. C. Rollings, J. Li, *et al.*, Controlling protein translocation through nanopores with bio-inspired fluid walls, *Nat. Nanotechnol.*, 2011, **6**(4), 253–260.

12 K. Hall, T. H. Lee, A. I. Mechler, M. J. Swann and M. I. Aguilar, Real-time measurement of membrane conformational states induced by antimicrobial peptides: balance between recovery and lysis, *Sci. Rep.*, 2014, **4**, 5479.

13 D. J. Hirst, T. H. Lee, M. J. Swann and M. I. Aguilar, Combined mass and structural kinetic analysis of multistate antimicrobial peptide-membrane interactions, *Anal. Chem.*, 2013, **85**(19), 9296–9304.

14 I. Reviakine, D. Johannsmann and R. P. Richter, Hearing what you cannot see and visualizing what you hear: interpreting quartz crystal microbalance data from solvated interfaces, *Anal. Chem.*, 2011, **83**(23), 8838–8848.

15 G. R. Heath, M. Li, I. L. Polignano, J. L. Richens, G. Catucci, P. O'Shea, *et al.*, Layer-by-Layer Assembly of Supported Lipid Bilayer Poly-L-Lysine Multilayers, *Biomacromolecules*, 2016, **17**(1), 324–335.

16 S. Shao, J. Geng, H. Ah Yi, S. Gogia, S. Neelamegham, A. Jacobs, *et al.*, Functionalization of cobalt porphyrin-phospholipid bilayers with his-tagged ligands and antigens, *Nat. Chem.*, 2015, **7**(5), 438–446.

17 T. T. Nguyen, K. L. Sly and J. C. Conboy, Comparison of the energetics of avidin, streptavidin, neutrAvidin, and anti-biotin antibody binding to biotinylated lipid bilayer examined by second-harmonic generation, *Anal. Chem.*, 2012, **84**(1), 201–208.

18 S. Vafaei, S. R. Tabaei, K. H. Biswas, J. T. Groves and N. J. Cho, Dynamic Cellular Interactions with Extracellular Matrix Triggered by Biomechanical Tuning of Low-Rigidity, Supported Lipid Membranes, *Adv. Healthcare Mater.*, 2017, **6**(10), 1700243.

19 M. R. Horton, C. Reich, A. P. Gast, J. O. Radler and B. Nickel, Structure and dynamics of crystalline protein layers bound to supported lipid bilayers, *Langmuir*, 2007, **23**(11), 6263–6269.

20 N. B. Eisele, F. I. Andersson, S. Frey and R. P. Richter, Viscoelasticity of thin biomolecular films: a case study on nucleoporin phenylalanine-glycine repeats grafted to a histidine-tag capturing QCM-D sensor, *Biomacromolecules*, 2012, **13**(8), 2322–2332.

21 T. G. Schmidt, L. Batz, L. Bonet, U. Carl, G. Holzapfel, K. Kiem, *et al.*, Development of the Twin-Strep-tag(R) and its application for purification of recombinant proteins from cell culture supernatants, *Protein Expression Purif.*, 2013, **92**(1), 54–61.

22 C. Garcia-Aljaro, F. X. Munoz and E. Baldrich, Captavidin: a new regenerable biocomponent for biosensing?, *Analyst*, 2009, **134**(11), 2338–2343.

23 A. Mashaghi, M. Swann, J. Popplewell, M. Textor and E. Reimhult, Optical anisotropy of supported lipid structures probed by waveguide spectroscopy and its application to study of supported lipid bilayer formation kinetics, *Anal. Chem.*, 2008, **80**(10), 3666–3676.

24 C. Song, P. Wang and H. A. Makse, A phase diagram for jammed matter, *Nature*, 2008, **453**(7195), 629–632.

25 C. Larsson, M. Rodahl and F. Hook, Characterization of DNA immobilization and subsequent hybridization on a 2D arrangement of streptavidin on a biotin-modified lipid bilayer supported on SiO_2, *Anal. Chem.*, 2003, **75**(19), 5080–5087.

26 M. M. Ouberai, K. Xu and M. E. Welland, Effect of the interplay between protein and surface on the properties of adsorbed protein layers, *Biomaterials*, 2014, **35**(24), 6157–6163.

27 C. Beggan and C. W. Hamilton, New image processing software for analyzing object size-frequency distributions, geometry, orientation, and spatial distribution, *Comput. Geosci.*, 2010, **36**(4), 539–549.

28 A. Gunnarsson, M. Bally, P. Jonsson, N. Medard and F. Hook, Time-resolved surface-enhanced ellipsometric contrast

imaging for label-free analysis of biomolecular recognition reactions on glycolipid domains, *Anal. Chem.*, 2012, **84**(15), 6538–6545.

29 D. Ausserre and M. P. Valignat, Surface enhanced ellipsometric contrast (SEEC) basic theory and lambda/4 multilayered solutions, *Opt. Express*, 2007, **15**(13), 8329–8339.

30 A. Ducret, M. P. Valignat, F. Mouhamar, T. Mignot and O. Theodoly, Wet-surface-enhanced ellipsometric contrast microscopy identifies slime as a major adhesion factor during bacterial surface motility, *Proc. Natl. Acad. Sci. U. S. A.*, 2012, **109**(25), 10036–10041.

31 A. M. Egea, E. Trevisiol and C. Vieu, Direct patterning of probe proteins on an antifouling PLL-g-dextran coating for reducing the background signal of fluorescent immunoassays, *Biointerphases*, 2013, **8**(1), 37.

32 S. Mun and S. J. Choi, Optimization of the hybrid bilayer membrane method for immobilization of avidin on quartz crystal microbalance, *Biosens. Bioelectron.*, 2009, **24**(8), 2522–2527.

33 E. Nileback, L. Feuz, H. Uddenberg, R. Valiokas and S. Svedhem, Characterization and application of a surface modification designed for QCM-D studies of biotinylated biomolecules, *Biosens. Bioelectron.*, 2011, **28**(1), 407–413.

34 N. S. Baranova, E. Nileback, F. M. Haller, D. C. Briggs, S. Svedhem, A. J. Day, *et al.*, The inflammation-associated protein TSG-6 cross-links hyaluronan via hyaluronan-induced TSG-6 oligomers, *J. Biol. Chem.*, 2011, **286**(29), 25675–25686.

35 M. Edvardsson, S. Svedhem, G. Wang, R. Richter, M. Rodahl and B. Kasemo, QCM-D and reflectometry instrument: applications to supported lipid structures and their biomolecular interactions, *Anal. Chem.*, 2009, **81**(1), 349–361.

36 H. Koldso, D. Shorthouse, J. Helie and M. S. Sansom, Lipid clustering correlates with membrane curvature as revealed by molecular simulations of complex lipid bilayers, *PLoS Comput. Biol.*, 2014, **10**(10), e1003911.

37 H. Zhan and T. Lazaridis, Inclusion of lateral pressure/curvature stress effects in implicit membrane models, *Biophys. J.*, 2013, **104**(3), 643–654.